Bexmarilimab Activates Human Tumor-Associated Macrophages to Support Adaptive Immune Responses in Interferon-Poor Immune Microenvironments

Jenna H. Rannikko[1], Petri Bono[2], Johanna Hynninen[3], and Maija Hollmén[1]

ABSTRACT

Immune checkpoint inhibitors (ICI) show substantially greater efficacy in inflamed tumors characterized by preexisting T-cell infiltration and IFN signaling than in noninflamed "cold" tumors, which often remain immunotherapy resistant. The cancer immunotherapy bexmarilimab, which inhibits the scavenger receptor Clever-1 to release macrophage immunosuppression and activate adaptive immunity, has shown treatment benefit in subsets of patients with advanced solid malignancies. However, the mechanisms that determine bexmarilimab therapy outcome in individual patients are unknown. Here we characterized bexmarilimab response in ovarian cancer ascites macrophages *ex vivo* using single-cell RNA sequencing and demonstrated increased IFN signaling and CXCL10 secretion following bexmarilimab treatment. We further showed that bexmarilimab was most efficacious in macrophages with low baseline IFN signaling, as chronic IFNγ priming abolished bexmarilimab-induced TNFα release. These results highlight an approach to target immunologically cold tumors and to increase the likelihood of their subsequent response to ICIs.

Introduction

Subsets of cancer patients develop durable clinical responses following treatment with immune checkpoint inhibitors (ICI), but these responses depend on preexisting T-cell infiltration and activation (1). To help patients unresponsive to ICIs, novel immunotherapies targeting the innate immune system are being developed (2, 3). Tumor-associated macrophages (TAM) are particularly attractive cancer immunotherapy targets given their high intratumoral abundance, continuous recruitment into tumors and aptness to functional reprogramming (4). Altering TAM function is essential, as these cells facilitate cancer growth and spread, limit antitumor T-cell responses, and suppress ICI therapy efficacy (5, 6). Noninflamed, immunologically "cold" tumors are especially rich in immunosuppressive immune cells, including TAMs, and lack T-cell infiltration and the pro-inflammatory cytokine environment (type I and II IFNs, IL12, and TNFα) typical to ICI response (7). Successful TAM-based therapies could limit protumoral TAM functions and engage innate immune cells to support adaptive immunity in the fight against cancer (3, 5).

Bexmarilimab is a humanized IgG4 antibody targeting the scavenger receptor Clever-1 (also known as Stabilin-1). Clever-1 regulates receptor-mediated endocytosis, intracellular sorting, and tolerance in monocytes, macrophages, and subsets of endothelial cells (8, 9). Disruption of monocyte and macrophage Clever-1 function enhances adaptive immune responses both in healthy and tumor-associated lymphocytes (10, 11). Functionally, bexmarilimab inhibits scavenging of modified LDL, reducing the activation of nuclear lipid receptors while promoting NF-κB activation. Upon binding to Clever-1, bexmarilimab is rapidly internalized into endosomes where it can hinder vacuolar ATPase-mediated lysosomal acidification and favor antigen presentation instead of degradation (12). The potential of targeting Clever-1 to induce antitumor immune responses is supported by early results from a first-in-human phase I/II trial (MATINS, FP-1305, https://clinicaltrials.gov/ct2/show/NCT03733990), which demonstrate activation of circulating monocytes and $CD8^+$ T cells after bexmarilimab therapy, and early signs of efficacy in patients with advanced solid tumors (12).

The mechanisms regulating bexmarilimab response at the individual patient level are presently unknown but clinically important to understand as emerging data reveals individual heterogeneity in responses to bexmarilimab. Here, we have characterized bexmarilimab activity in the human tumor immune microenvironment (TIME) using *ex vivo*–treated ovarian cancer ascites cells. We found bexmarilimab enhanced IFN signaling and T-cell chemotaxis in TAMs lacking previous exposure to IFNs and thus provide proof-of-concept for bexmarilimab as a therapeutic capable of activating antitumoral immunity in immunologically cold tumors.

Methods

Patient samples

Ascites was collected from ovarian cancer patients (Supplementary Table S1) with the approval of The Ethics Committee of the Hospital District of Southwest Finland (license numbers ETMK 53/1801/2009 and ETMK 145/1801/2015) and in accordance with the ethical principles of the Declaration of Helsinki. Written informed consent was obtained from each participant.

Tumor biopsies were obtained from participants of the first-in-human phase I/II MATINS trial investigating bexmarilimab therapy (13). The trial was run according to Good Clinical Practice and the Declaration of Helsinki, and approved by local institutional review boards and national medicinal agencies (NCT03733990, EudraCT 2018–002732–24); written informed consents were obtained from the participants. The biopsies were collected from December 2018 to June 2021 and stored at 4°C until use. Pretreatment biopsies used in this

[1]MediCity Research Laboratory and InFLAMES Flagship, University of Turku, Turku, Finland. [2]Terveystalo, Helsinki, Finland. [3]Department of Obstetrics and Gynecology, University of Turku and Turku University Hospital, Turku, Finland.

Corresponding Author: Maija Hollmén, MediCity Research Laboratory, University of Turku, Tykistökatu 6A, Turku 20520, Finland. E-mail: maijal@utu.fi

Cancer Immunol Res 2024;12:48–59

doi: 10.1158/2326-6066.CIR-23-0350

study were collected from patients with advanced (inoperable or metastatic), treatment-refractory and histologically confirmed gastric adenocarcinoma, hepatocellular carcinoma, gallbladder or biliary tract carcinoma, estrogen receptor–positive breast cancer or ICI-refractory cutaneous melanoma (Supplementary Table S2). The patients were categorized as DCR (disease control) or non-DCR (no disease control) based on the presence of RECIST 1.1–defined disease control at cycle 4 of bexmarilimab therapy.

Ovarian ascites cell culture and bexmarilimab treatment

Ascites samples were collected from December 2010 to November 2011 and from October 2019 to November 2020. Ascites fluid from patients with ovarian cancer (50–190 mL) was centrifuged at 400 *g* for 10 minutes at room temperature and the resulting pellet was subjected to red blood cell lysis with PharmLyse (BD Biosciences, catalog no. 555899). Cells were washed with RPMI-1640 (Sigma, catalog no. 5886) supplemented with 10% FCS (Sigma, catalog no. F7524), 1% GlutaMAX (Gibco, catalog no. 35050–038), and penicillin-streptomycin (P/S, 12,8 U/mL, Gibco, catalog no. 15140–122), and then frozen in the same medium additionally supplemented with 10% DMSO. Frozen ascites cells were stored at −150°C until use.

For bexmarilimab treatment, ascites cells were thawed and washed with RPMI supplemented with 10% FCS, 1% GlutaMAX, and P/S. In some experiments, monocytes/macrophages (MoMacs) were magnetically enriched by using human $CD14^+$ MicroBeads (Miltenyi Biotec, catalog no. 130–050–201) according to the manufacturer's instructions. All ascites cells (0.5×10^6) or $CD14^+$ cells (0.2×10^6) were plated in IMDM (Gibco, catalog no. 21980–032) supplemented with 10% FCS, 1% GlutaMAX, and P/S on an ultralow attachment plate (Corning, catalog no. 7007) with 10 μg (all cells) or 15 μg ($CD14^+$ cells) of antibodies. The antibodies used were bexmarilimab (FP-1305; clone CP12, Abzena) and its isotype control IgG4 (human irrelevant IgG4 (S241P, L248E), Abzena). After 48 hours of antibody treatment at 37°C, 5% CO_2, the plate was centrifuged at 340 *g* for 3 minutes at room temperature. Cell culture supernatants were collected and frozen for cytokine profiling with Bio-Plex (see *Multiplex immunoassay for cytokine profiling*). For qPCR, ascites cells were washed once with PBS + 0.5% FCS + 2 mmol/L EDTA, resuspended in 800 μL TRIsure (Bioline, catalog no. BIO-38032) and stored at −70°C until RNA extraction. Alternatively, treated ascites cells were collected for single-cell RNA sequencing (scRNA-seq) by first collecting the cells in suspension and then combining these cells with the remaining cells that were detached with 10 mmol/L EDTA. Collected cells were washed twice with 0.04% BSA-PBS and filtered through 70-μm nylon nets (Corning, catalog no. 352350). The resulting single-cell suspensions were prepared for scRNA-seq (see *scRNA-seq*).

RNA extraction for qPCR

RNA was extracted from treated ascites cells according to the manufacturer's protocol for TRIsure (Bioline, catalog no. BIO-38032). Thawed samples were mixed with 200 μL chloroform and centrifuged at 12,000 *g* for 15 minutes at 4°C. Aqueous phase containing the RNA was collected, precipitated with 500 μL cold isopropyl alcohol for 10 minutes at room temperature and samples centrifuged at 12,000 *g* for 10 minutes at 4°C. Pellets were washed once with 1 mL 75% ethanol, air-dried and dissolved in nuclease-free water (Ambion, catalog no. AM9930). RNA quantity was measured with Qubit Flex Fluorometer using Qubit HS Assay kit (both Thermo Fisher, kit catalog no. Q32852) and quality was analyzed with Bioanalyzer (Agilent) using RNA 6000 Pico kit (Agilent, catalog no. 5067–1513) following the manufacturers' protocols.

qPCR

RNA (150 ng per sample or otherwise equal quantity across patient's samples) was reverse-transcribed into cDNA using SuperScript VILO cDNA Synthesis Kit (ThermoFisher, catalog no. 11754–250) in 20 μL reactions according to the kit's protocol. For qPCR, triplicate reactions (10 μL) were prepared on a 96-well plate (4titude Biotop UK, catalog no. 4ti-0770/c) containing 7.5 ng of cDNA, 5 μL Taqman universal master mix II, no UNG (ThermoFisher, catalog no. 4427788), and 0.25 μL Taqman gene expression assay. The following Taqman Assays (ThermoFisher, catalog no. 4331182) were used: *CIITA* (Hs00172106_m1), *MX1* (Hs00895608_m1), and *GAPDH* (Hs02758991_g1). Reactions were run on QuantStudio3 (Applied Biosystem) using QuantStudio Design and analysis software (v1.5.1 Applied Biosystems) with following cycling conditions: 1 × 10 minutes at 95°C, 40 × 15 seconds at 95°C and 1 minutes at 60°C. Relative quantification was calculated with the ΔΔCT method using *GAPDH* as the endogenous control and bexmarilimab fold changes were calculated in relation to the IgG4-treated samples.

scRNA-seq

Filtered ovarian ascites cells were re-suspended in freshly-prepared 0.04% ultrapure BSA-PBS (ThermoFisher, catalog no. AM2616) and single-cell library preparation was conducted at Single Cell Omics Facility at Turku Bioscience Center. Briefly, single-cell partitioning with Chromium Controller and scRNA-seq library preparation were done using Chromium Next GEM Single Cell 3′ GEM Library & Gel Bead Kit v3.1 and Chromium Next GEM Chip G Single Cell Kit (10X Genomics) according to the manufacturer's protocols. Single indexes were used for batch 1 (Protocol: CG000204 Rev D), and dual indexes for batch 2 (Protocol: CG000315 Rev E). Full-length cDNA was amplified by PCR (Veriti, Applied Biosystems) and cleaned using SPRIselect Reagent Kit (Beckman Coulter, catalog no. B23318). Amplified cDNA was fragmented, end-repaired and A-tailed prior to sample index PCR. The libraries were sequenced using an Illumina NovaSeq 6000 instrument with an S2 flow cell and following read length configurations: R1 = 29, i7 = 8, i5 = 0 and R2 = 92 (Batch 1); R1 = 28, i7 = 10, i5 = 10, R2 = 90 (Batch 2). Data post-processing including demultiplexing, read alignment and quality control were performed using Cell Ranger package (v5.0.1 and v6.1.1, 10X Genomics) with GRCh38 as the reference genome.

scRNA-seq data analysis

Four bexmarilimab-responsive (R) and nonresponsive (NoR) ovarian ascites cell samples were selected on the basis of *MX1* induction measured by qPCR, treated with bexmarilimab or IgG4 and analyzed by scRNA-seq. After scRNA-seq, one NoR sample was excluded from further analyses due to low scRNA-seq data quality. scRNA-seq data from the seven remaining patients was analyzed using Seurat (v4.0.1; ref. 14). Default settings were used, unless otherwise indicated.

Dead cells were excluded by filtering out cells with >13% mitochondrial RNA and <1,100 unique expressed genes. Doublet cells were identified using DoubletFinder package (v2.0.3; ref. 15). Briefly, paramSweep_v3 (PCs = 1:20, sct = T), summarizeSweep and find.pK functions were used to find pK values. pK value less than 0.1 and corresponding to highest BCmetric peak was chosen for each sample. Expected doublet formation rate of 7.6% was assumed on the basis of the target number of recovered cells (10,000). Doublets were identified with doubletFinder_v3 (PCs = 1:20, pN = 0.25, sct = T) using pK and nExp values chosen as described above, and then excluded from further analyses. Next, we merged each patient's bexmarilimab- and IgG4-treated sample and integrated resulting seven samples by using

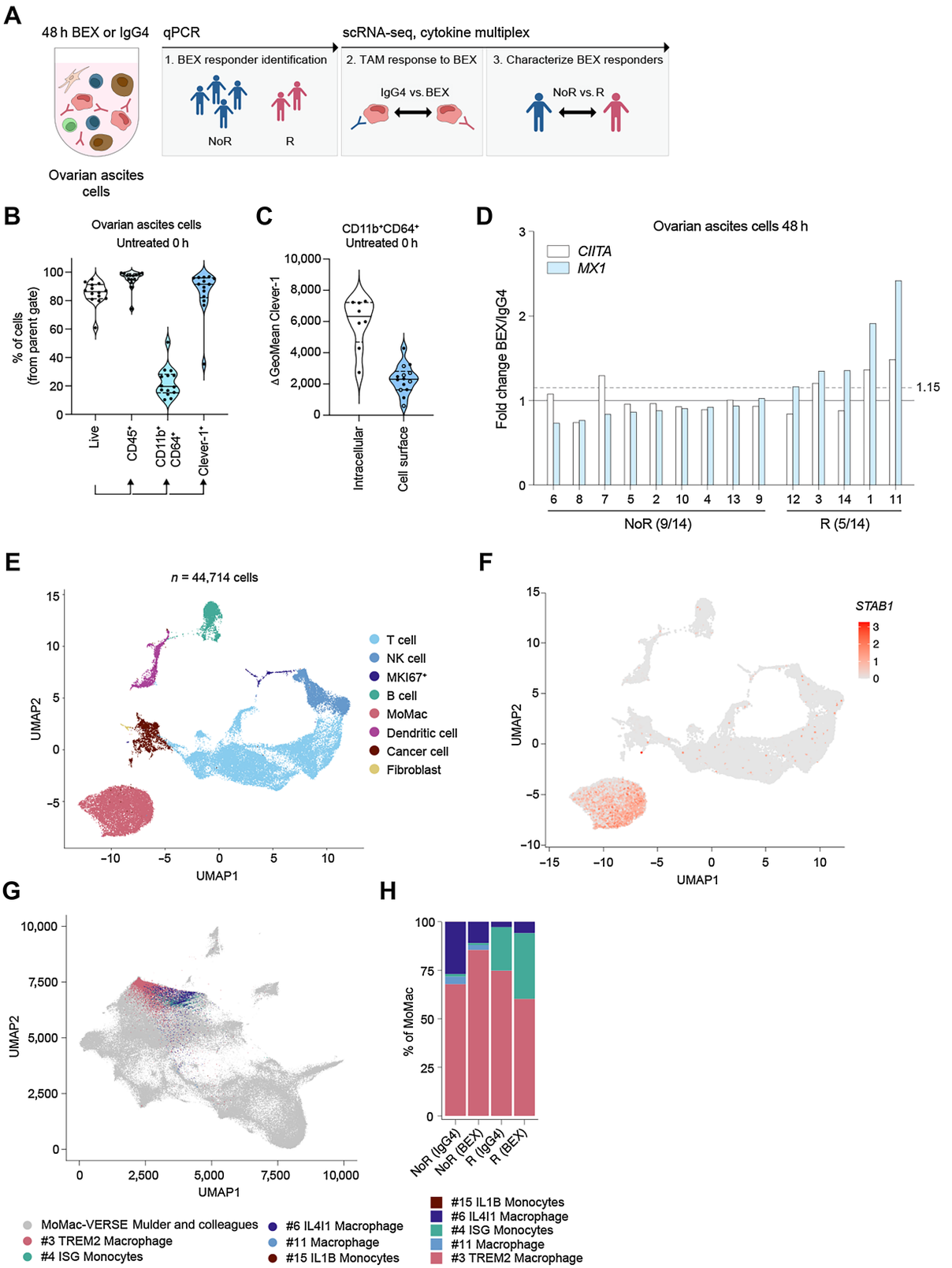
A
48 h BEX or IgG4
qPCR
scRNA-seq, cytokine multiplex
1. BEX responder identification
2. TAM response to BEX
3. Characterize BEX responders
NoR
R
IgG4 vs. BEX
NoR vs. R
Ovarian ascites cells
B
Ovarian ascites cells
Untreated 0 h
% of cells (from parent gate)
Live
CD45+
CD11b+ CD64+
Clever-1+
C
CD11b+CD64+
Untreated 0 h
Δ GeoMean Clever-1
Intracellular
Cell surface
D
Ovarian ascites cells 48 h
CIITA
MX1
Fold change BEX/IgG4
1.15
6 8 7 5 2 10 4 13 9
12 3 14 1 11
NoR (9/14)
R (5/14)
E
n = 44,714 cells
T cell
NK cell
MKI67+
B cell
MoMac
Dendritic cell
Cancer cell
Fibroblast
UMAP1
UMAP2
F
STAB1
G
MoMac-VERSE Mulder and colleagues
#3 TREM2 Macrophage
#4 ISG Monocytes
#6 IL4I1 Macrophage
#11 Macrophage
#15 IL1B Monocytes
H
% of MoMac
NoR (IgG4)
NoR (BEX)
R (IgG4)
R (BEX)
#15 IL1B Monocytes
#6 IL4I1 Macrophage
#4 ISG Monocytes
#11 Macrophage
#3 TREM2 Macrophage

functions SCTransform (vars.to.regress = "percent.mt"), SelectIntegrationFeatures (nfeatures = 3000), PrepSCTIntegration, FindIntegrationAnchors (normalization.method = "SCT") and IntegrateData (normalization.method = "SCT", dims = 1:50). Integrated data was clustered using functions RunPCA (npcs = 100), RunUMAP (dims = 1:60), FindNeighbors (dims = 1:60) and FindClusters (resolution = 0.1). MoMacs and dendritic cells (DC) were subclustered together (dims = 1:30, resolution = 0.5) and a monocyte-derived DC cluster was identified within the MoMac main cluster and merged with rest of the DCs for subclustering. Natural killer (NK) cells and T cells (dims = 1:35, resolution = 1), B cells (dims = 1:30, resolution = 0.5), DCs (dims = 1:30, resolution = 2), and MoMacs (dims = 1:30, resolution = 1) were subclustered by repeating integration and clustering as described above. A LYZ^+ NKT subcluster and $CD3E^+$ B-cell subcluster were excluded from the analyses as doublets. Log-normalized counts of the RNA assay were used in calculating the proportion of CXCL10-expressing MoMacs, visualizing the expression of individual genes on uniform manifold approximation and projection (UMAP) plots and plotting the average expression of cluster marker genes, monocyte-derived DC marker genes (16, 17) and myeloid-derived suppressor cell (MDSC) marker genes (18, 19).

MoMacs were mapped into a monocyte and macrophage cross-tissue single-cell atlas, MoMac-VERSE (20). Before mapping, our MoMac data was split into original sample objects, merged by scRNA-seq experiment batch and normalized (NormalizeData). Seurat's reference mapping functions FindTransferAnchors (dims = 1:100, npcs = 100, reference.reduction = "pca", query.assay = "RNA") and MapQuery (reduction.model = "umap") were used to map our MoMacs on MoMac-VERSE UMAP embeddings and to transfer cluster labels from MoMac-VERSE. Mapped MoMacs were visualized on MoMac-VERSE UMAP after merging the reference and mapped datasets. MoMac-VERSE cluster labels of mapped cells were used in further analyses. Mapping was done separately for the two scRNA-seq experiment batches, because this method yielded higher median prediction.scores for samples and MoMac-VERSE clusters.

For analyzing bexmarilimab-induced changes in gene expression, gene set enrichment analysis (GSEA) was used. First, we randomly subsetted each sample to a maximum of 500 MoMacs or 500 $CD8^+$ T cells and created pseudobulk samples from these cells by summarizing their counts data. Pseudobulk samples were normalized using DESeq2 (v1.30.1, function: estimateSizeFactors). Normalized count matrix and sample phenotype files containing information on antibody treatment, patient and bexmarilimab response group were loaded into GSEA software (v4.1.0, Broad Institute). Gene set enrichment was analyzed between indicated samples or sample groups using Hallmarks gene set collection (h.all.v7.4.symbols.gmt), 1,000 permutations of gene sets, ensemble gene IDs and otherwise default settings.

For comparing immune cell constitution of ascites samples, we calculated percentages of MoMacs, DCs, NK cells, T cells, and B cells from $CD45^+$ cells and percentages of all immune cell subclusters and MoMac phenotypes from their corresponding main $CD45^+$ cell cluster. This resulted in a total of 38 parameters, which were used in clustering of patients by principal component analysis (PCA) and unsupervised hierarchical clustering. PCA was performed and visualized as a 3D scatter plot using JMP Pro software (v16.2.0). Samples were hierarchically clustered on the basis of scaled and centered cell percentages (R v4.0.4, Euclidean distance, complete linkage) and resulting dendrograms plotted together with a heat map using ComplexHeatmap package (v2.6.2) (21).

Multiplex immunoassay for cytokine profiling

Cytokine levels in ascites cell and $CD14^+$ ascites cell culture supernatants were measured using Bio-Plex Pro Human Cytokine 27-plex assay (Bio-Rad, catalog no. M500KCAF0Y) and Bio-Plex 200 System (Bio-Rad) according to the manufacturer's instructions. Cytokines with >10% of datapoints outside the detection range were excluded from the analyses. Remaining values lower than the detection limit were replaced by 0.5 × lowest measured value. Results are presented as fold changes between bexmarilimab- and IgG4-treated samples.

Primary human macrophage and monocyte-derived DC culture

Monocytes were obtained from EDTA blood of healthy volunteer donors under the approval of The Ethics Committee of the Hospital District of Southwest Finland (license number ETMK 43/1801/2015). Peripheral blood mononuclear cells were isolated using Ficoll-Paque Plus (Cytiva, catalog no. 17–1440–03) density gradient centrifugation and further magnetically enriched for monocytes using human CD14 MicroBeads (Miltenyi Biotec, catalog no. 130–050–201) as instructed by the manufacturer. Monocytes (0.7×10^6) were cultured on 6-well plates (Greiner, catalog no. 657160) in IMDM supplemented with 10% FCS and 1% GlutaMAX at 37°C and 5% CO_2. For macrophage differentiation, the medium was supplemented with 50 ng/mL recombinant human M-CSF (BioLegend, catalog no. 574806) and for monocyte-derived DC (mo-DC) differentiation the medium was supplemented with 500 U/mL human GM-CSF (PeproTech, catalog no. 300–23) and 350 U/mL human IL4 (PeproTech, catalog no. 200–04). Half of the culture medium was replenished every two days. After 6 days, macrophage culture media were further supplemented with dexamethasone (100 nmol/L, Sigma, catalog no. D2915) and IL4 (20 ng/mL, PeproTech, catalog no. 200–04) to polarize the macrophages toward an M2 phenotype. After 24 hours of polarization, macrophages and mo-DCs were detached for flow cytometry staining by a 20-minute incubation in 10 mmol/L EDTA at 37°C and subsequent gentle scraping.

For IFN priming, monocytes were differentiated in the aforementioned macrophage differentiation medium for 96 hours and then detached as described above. Indicated concentrations of recombinant human IFNα2 (BioLegend, catalog no. 592702) or recombinant human IFNγ (PeproTech, catalog no. AF-300–02) were added at

Figure 1.
Profiling of bexmarilimab responses in ovarian ascites TAMs with scRNA-seq. **A,** Characterization of bexmarilimab responses and responding patients in ovarian ascites cells. **B,** Flow cytometry staining of untreated ovarian ascites cells ($n = 14$ patients). Violin plots show proportions of live cells, $CD45^+$ immune cells, $CD11b^+CD64^+$ MoMacs and Clever-1^+ cells (median and quartiles). Percentages were calculated from the parent gate and Clever-1 expression measured from the cell surface. **C,** Total ($n = 8$) and cell surface ($n = 14$) Clever-1 expression on $CD11b^+CD64^+$ ovarian ascites cells. Open circles represent patients with cell surface staining only. **D,** Change in *MX1* and *CIITA* gene expression measured by qPCR from ovarian ascites cells treated with bexmarilimab or IgG4 for 48 hours. The dashed line indicates *MX1* cutoff for responder identification and fractions indicate proportions of R and NoR patients. **E,** scRNA-seq of ovarian cancer ascites cells ($n = 7$ patients) treated *ex vivo* with bexmarilimab or IgG4 for 48 hours. UMAP dimensionality reduction of cells colored by main cell type clusters. **F,** UMAP colored by Clever-1 expression (*STAB1*). **G,** Mapping of monocytes and macrophages ($n = 10{,}358$ cells) to MoMac-VERSE atlas created by Mulder and colleagues. Original MoMac-VERSE UMAP plot is colored in gray and mapped cells colored by MoMac-VERSE clusters. **H,** Bar graph showing percentage of ovarian ascites monocytes and macrophages mapped to each MoMac-VERSE cluster (R, $n = 4$; NoR, $n = 3$ patients). BEX, bexmarilimab; IgG4, isotype control for bexmarilimab.

the time of monocyte plating or 2 hours prior to detaching the macrophages. Macrophages (2×10^4) were re-plated on flat-bottom 96-well plates (Greiner, catalog no. 655–180) in triplicates in IMDM supplemented with 10% FCS and 1% GlutaMAX as well as 10 μg/mL bexmarilimab or IgG4 and with or without IFN. After the 24 hours of antibody treatment, the cells were washed with PBS and then 20 ng/mL TLR4-specific LPS (InvivoGen, #tlrl-3pelps) was added in fresh macrophage differentiation medium for 12 hours. Finally, cell culture medium from triplicate wells was collected and combined, centrifuged at 2,000 *g* for 5 minutes at 4°C and frozen for subsequent analysis by ELISA. Plates were frozen at −70°C for cell number quantification.

ELISA

Macrophage secretion of TNFα was measured from cell culture supernatants using TNF alpha Human ELISA Kit (ThermoFisher, catalog no. KHC3011) according to the manufacturer's instructions. The standard curve was fitted using a sigmoidal 4PL curve (x = concentration) with GraphPad Prism (v9.2.0) software. Obtained concentrations were further normalized to cell numbers in the wells by measuring well DNA and RNA quantity using CyQUANT Cell Proliferation Assay Kit (ThermoFisher, catalog no. C7026). The CyQUANT Cell Proliferation Assay Kit's DNA standard curve was used for removing plate-to-plate variation per kit's instructions.

Flow cytometry

Thawed ascites cells (1×10^6 [surface stain], 2.5×10^6 [intracellular stain]), IFN-primed macrophages (5×10^4) or macrophages/mo-DCs (1×10^5) were plated in round-bottom 96-well plates and washed with PBS. Ascites cells were stained with Fixable Viability Dye eFluor 780 (Invitrogen, catalog no. 65–0865–14, 1:1,000) in PBS for 20 minutes at 4°C, followed by a PBS wash. For cell surface staining, unspecific binding was blocked by a 15-minute incubation with 0.2 mg/mL Kiovig (Baxter, catalog no. LE-072213) and cells were stained for 30 minutes at 4°C. The staining and two washes after the staining were performed with PBS + 2% FCS + 0.01% NaN_3.

Intracellular staining was performed for ascites cells stained with Viability dye eFluor 780 and surface markers, IFN-primed macrophages stained with Fixable Viability Dye eFluor 450 (Invitrogen, catalog no. 65–0863–14, 1:1,000) and macrophages/mo-DCs (1×10^5). These cells were fixed with 4% PFA for 15 minutes at room temperature, washed twice with PBS, and permeabilized with 0.3% tween-20 in PBS for 20 minutes at room temperature. This was followed by a wash with PBS + 2% FCS + 0.01% NaN_3. Cells were blocked with Kiovig for 15 minutes at room temperature and stained in PBS + 2% FCS + 0.01% NaN_3 for 30 minutes at room temperature, followed by two washes.

Antibodies used in ascites cell staining were: anti-human CD45 BV421 (clone H130, BD Biosciences, catalog no. 563879, 1:100), anti-human CD11b AF488 (clone ICRF44, Biolegend, catalog no. 301318, 1:100), anti-human CD64 BV510 (clone 10.1, BD Biosciences, 563459, 1:100), bexmarilimab AF647 (20 μg/mL) or its isotype control IgG4 AF647 (clone QA16215, BioLegend, catalog no. 403702, 20 ug/mL), and anti-Clever-1 AF647 (clone 9–11, InVivo, 10 μg/mL) or its isotype control rat IgG2a AF647 (clone R35–95, BD Biosciences, catalog no. 557906, 1:100). Antibodies used in primary macrophage and mo-DC staining were: IDO1 PE (clone eyedio, ThermoFisher, catalog no. 12–9477–42, 1:133), bexmarilimab AF647 (20 μg/mL) or IgG4 AF647 (20 μg/mL), anti-Clever-1 AF488 (clone 9–11, InVivo, 10 μg/mL) or rat IgG2a AF488 (clone MEL-14, InVivo, 10 μg/mL). Anti-Clever-1 antibodies were conjugated in-house to Alexa Fluor (AF) 647 or AF488 using Alexa Fluor Protein Labeling kits (ThermoFisher, catalog no. A20173 and A10235) according to the manufacturer's instructions.

Stained cells were kept in PBS with 1% formaldehyde at 4°C and analyzed with an LSRFortessa (BD). Acquired data from single-stained UltraComp eBeadsTM Compensation Beads (Invitrogen, catalog no. 01–2222–42) and viability dye-stained cells were used to correct for fluorochrome spectral overlap. Data were analyzed with FlowJo (v10.8.1, BD). Ascites monocytes and macrophages were identified as ViabilityDye$^-$CD45$^+$CD11b$^+$CD64$^+$.

IHC

Formalin-fixed, paraffin-embedded (FFPE) tissue sections from MATINS trial pretreatment biopsies were deparaffinized and subjected to heat-mediated antigen retrieval in Tris-EDTA (pH 9.0). Endogenous peroxidase activity was blocked with BLOXALL (Vector Laboratories, catalog no. SP-6000) for 15 minutes at room temperature. Sections were stained using Vectastain Elite ABC-HRP kit (rabbit IgG, Vector laboratories, PK-6101). After blocking with normal goat serum (1 hour at room temperature), sections were stained with anti-human IL4I1 (clone EPR22070, abcam, catalog no. ab222102, 1:2,000) and rabbit IgG (polyclonal, BioXCell, catalog no. BE0095) overnight at 4°C. Biotinylated secondary antibody and ABC reagent were used according to the kit's instructions. The rabbit IgG staining was detected with 3,3′-diaminobenzidine (DAB, Dako, catalog no. K3468) as substrate. For double staining, FFPE breast cancer tumor sections were further stained with CD68 AF647 (clone KP-1, Santa-Cruz, catalog no. sc20060) or isotype control mouse IgG1 κ AF647 (clone MPC-21, BD, catalog no. 557783) for 1h at room temperature. Finally, sections were mounted in ProLong Gold antifade mountant (Invitrogen). Images of IL4I1 single staining were captured with Pannoramic P1000 slide scanner (3D Histech) using a 20X objective. Images of IL4I1 and CD68 double staining were captured sequentially with fluorescence and brightfield configurations on Nikon Eclipse Ti2-E connected to ORCA-Flash4.0 (Hamamatsu) and DC-Fi3 (Nikon) cameras using a 20x objective (Nikon CFI Plan Apo λ, NA 0.75).

IHC image analysis

Double-staining for IL4I1 and CD68 was analyzed using Fiji software (v1.53q, NIH). Fluorescence images were scaled to have equal pixel densities with the brightfield images. Fluorescence images of CD68 staining were thresholded, converted into binary masks and the masks were further modified by closing, filling holes and filtering out particles smaller than cells. Outlines of the resulting masks were displayed on top of the IL4I1 brightfield images to show colocalization of IL4I1 with CD68$^+$ cells.

For analyzing the density of IL4I1$^+$ cells in the stroma of pretreatment tumor biopsies (n = 45; DCR = 13 and non-DCR = 32), obtained .MRSX files were imported into QuPath v0.4.3 (22) and biopsy regions annotated. As IL4I1 (DAB) was the only chromogen on the sections, optical density sum of the three RGB channels was used in analyses to represent IL4I1 staining. Because the levels of IL4I1 staining on tumor cells and background signal varied highly between sections, we categorized samples into four analysis groups based on IL4I1 staining intensity that was measured as an average from three regions around the sections. Quartile values were used to create the four intensity groups, and we verified that each intensity group comprised of both DCR and non-DCR patients. While all analysis steps were performed similarly for each group, threshold values were adjusted for each group separately to allow better IL4I1$^+$ cell detection. IL4I1$^+$ cells

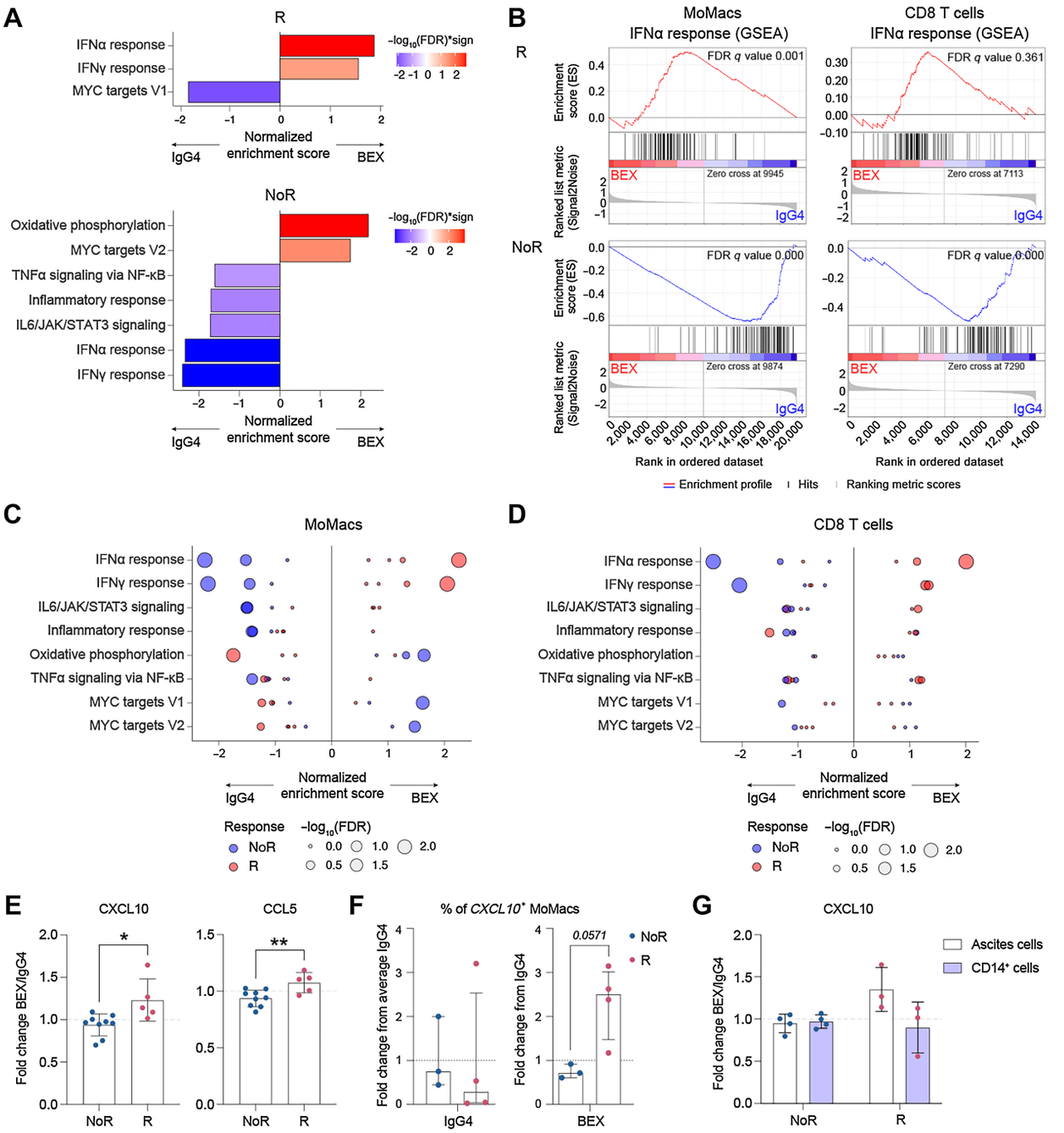

Figure 2.

Bexmarilimab triggers IFN signaling and CXCL10 secretion in subsets of ovarian ascites TAMs. **A,** Bexmarilimab-induced changes in MoMac gene expression were analyzed by a GSEA separately in R ($n = 4$) and NoR ($n = 3$) group. Significantly altered pathways (FDR-adjusted q-value < 0.05) are shown. Red color indicates pathway upregulation by bexmarilimab treatment and blue color pathway downregulation. **B,** Enrichment plots showing IFNα response gene enrichment after bexmarilimab treatment separately in MoMacs and CD8$^+$ T cells. Positive peaks indicate pathway upregulation and negative peaks downregulation. **C** and **D,** For significantly altered pathways presented in **Fig. 2A**, GSEA results from MoMacs (**C**) and CD8$^+$ T cells (**D**) are displayed separately in each patient. Positive normalized enrichment scores indicate pathway upregulation by bexmarilimab, and negative score pathway downregulation. Dot color marks bexmarilimab response group and dot size increases with higher significance. **E,** Fold changes in indicated cytokines were measured from ovarian ascites cell culture supernatants after 48 hours of bexmarilimab treatment ($n = 14$ patients). Mean ± SD; unpaired t test; *, $P < 0.05$; **, $P < 0.01$. **F,** Percentage of *CXCL10* expressing MoMacs was analyzed by scRNA-seq after 48 hours of IgG4 or bexmarilimab treatment. Median ± IQR, Mann–Whitney U test (NoR, $n = 3$; R, $n = 4$ patients). The bars correspond to following *CXCL10*$^+$ MoMac proportions: 16.5% (NoR IgG4), 6.4% (R IgG4), 15.1% (NoR BEX) and 16.6% (R BEX). **G,** Fold change in CXCL10 was measured from ascites cell or CD14$^+$ ascites cell culture supernatants after 48 hours of bexmarilimab treatment. Mean ± SD (NoR, $n = 5$; R, $n = 3$ patients). BEX, bexmarilimab; IgG4, isotype control for bexmarilimab.

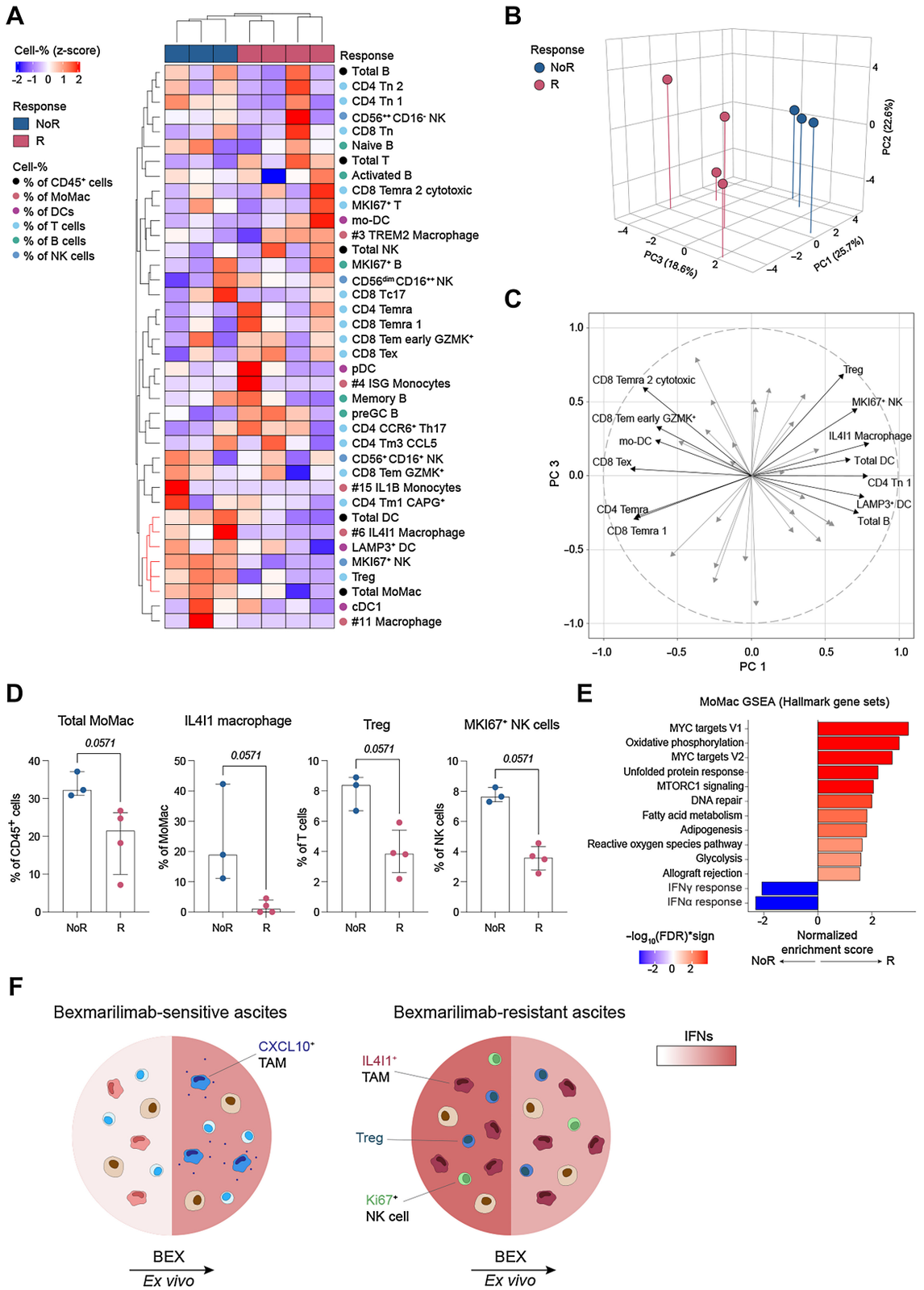
A
Cell-% (z-score)
-2 -1 0 1 2
Response
NoR
R
Cell-%
% of CD45+ cells
% of MoMac
% of DCs
% of T cells
% of B cells
% of NK cells
Response
Total B
CD4 Tn 2
CD4 Tn 1
CD56++ CD16- NK
CD8 Tn
Naive B
Total T
Activated B
CD8 Temra 2 cytotoxic
MKI67+ T
mo-DC
#3 TREM2 Macrophage
Total NK
MKI67+ B
CD56dim CD16++ NK
CD8 Tc17
CD4 Temra
CD8 Temra 1
CD8 Tem early GZMK+
CD8 Tex
pDC
#4 ISG Monocytes
Memory B
preGC B
CD4 CCR6+ Th17
CD4 Tm3 CCL5
CD56+ CD16+ NK
CD8 Tem GZMK+
#15 IL1B Monocytes
CD4 Tm1 CAPG+
Total DC
#6 IL4I1 Macrophage
LAMP3+ DC
MKI67+ NK
Treg
Total MoMac
cDC1
#11 Macrophage
B
Response
NoR
R
PC2 (22.6%)
PC1 (25.7%)
PC3 (18.6%)
C
CD8 Temra 2 cytotoxic
Treg
MKI67+ NK
CD8 Tem early GZMK+
IL4I1 Macrophage
mo-DC
Total DC
CD8 Tex
CD4 Tn 1
LAMP3+ DC
CD4 Temra
Total B
CD8 Temra 1
PC 3
PC 1
D
Total MoMac
IL4I1 macrophage
Treg
MKI67+ NK cells
0.0571
% of CD45+ cells
% of MoMac
% of T cells
% of NK cells
NoR
R
E
MoMac GSEA (Hallmark gene sets)
MYC targets V1
Oxidative phosphorylation
MYC targets V2
Unfolded protein response
MTORC1 signaling
DNA repair
Fatty acid metabolism
Adipogenesis
Reactive oxygen species pathway
Glycolysis
Allograft rejection
IFNγ response
IFNα response
-log10(FDR)*sign
Normalized enrichment score
NoR
R
F
Bexmarilimab-sensitive ascites
Bexmarilimab-resistant ascites
IFNs
CXCL10+ TAM
IL4I1+ TAM
Treg
Ki67+ NK cell
BEX
Ex vivo

were detected using QuPath's Cell detection tool with following settings: 20 μm background radius, 1 μm median filter radius, 1.5 μm sigma, 20 μm^2 minimum area, 400 μm^2 maximum area, cell expansion and splitting of shapes disabled and threshold value optimized for each analysis group. Stromal area was annotated by first detecting IL4I1$^+$ tumor cell area (Create thresholder with a threshold determined by visual inspection, minimum object size 500 μm^2 and minimum hole size 100 μm^2) and then inverting the obtained tumor area mask. Number of detections (IL4I1$^+$ cells within the stromal area) and stromal area were exported and results reported as IL41$^+$ stromal cells per mm^2 of stroma. Patients with poor stromal area detection ($n = 7$; of which DCR = 1) or poor-quality biopsies ($n = 5$; of which DCR = 2) were excluded from the analysis.

Statistical analysis

Statistical analysis was performed and graphs created using GraphPad Prism (v9.2.0, GraphPad Software) or R (v4.0.4, R Core Team) software. All data are presented mean ± SD unless otherwise indicated. For comparing two groups, *t* test (unpaired or paired) or Mann–Whitney U test was used for normally and non-normally distributed data, respectively. To compare multiple groups of matched data, repeated measurements one-way ANOVA was used. For analyzing each groups' deviance from baseline, one-sample *t* test was used. $P < 0.05$ was considered statistically significant.

Availability of data

The scRNA-seq data generated in this study is publicly available in Gene Expression Omnibus at GSE222649. All other data generated in this study are available within the article and its Supplementary Data files or from the corresponding author upon reasonable request. MoMac-VERSE with UMAP reduction.model was kindly provided by Mulder and colleagues. The data is otherwise same as MoMac-VERSE found at https://github.com/gustaveroussy/FG-Lab

Results

Ovarian ascites is rich in Clever-1$^+$ TAMs and responsive to bexmarilimab treatment

We set out to characterize the bexmarilimab-responsive TIME by studying bexmarilimab activity *ex vivo* in ovarian cancer ascites cells collected from patients participating in the DECIDER project (https://www.deciderproject.eu/; **Fig. 1A**; Supplementary Table S1). The ovarian ascites cell suspensions were rich in immune cells and Clever-1–expressing MoMacs (**Fig. 1B**; Supplementary Fig. S1A). Clever-1 expression on MoMacs showed patient-to-patient heterogeneity (**Fig. 1C**; Supplementary Fig. S1B), and it was not significantly altered by *ex vivo* bexmarilimab or isotype control IgG4 treatment (Supplementary Fig. S1C–S1E). Reflecting the observed increase in systemic IFNγ in a subset of bexmarilimab-treated patients (12) we measured the induction of two IFN-regulated genes, *MX1* (induced by type I IFNs) and *CIITA* (induced by type II IFNs), as a positive readout for bexmarilimab response in the ascites samples. Both genes were upregulated primarily in the same ascites samples, but *MX1* more strongly than *CIITA*. We found *MX1* upregulation (>1.15-fold change) in 36% of the treated ascites samples, which we classified as bexmarilimab-responsive (R; **Fig. 1D**).

For a more detailed analysis of the effect of bexmarilimab on Clever-1$^+$ MoMacs and surrounding immune cells, we analyzed *ex vivo*–treated samples classified as bexmarilimab R or NoR by scRNA-seq. High-quality single-cell data from seven *ex vivo*–treated ascites samples (R: $n = 4$; NoR: $n = 3$) were integrated and annotated by the main cell types (**Fig. 1E**; Supplementary Fig. S2). Clever-1 was highly and selectively expressed on the MoMac cluster (*STAB1*, **Fig. 1F**). This cluster comprised mainly of monocytes and macrophages, with a small contribution of mo-DCs (Supplementary Fig. S3A) that were subsequently analyzed alongside other DCs. While mo-DCs showed *STAB1* expression based on our scRNA-seq data, Clever-1 protein levels and bexmarilimab epitope availability were markedly lower on the surface of *in vitro*–cultured mo-DCs than M2 macrophages (77% and 94% lower on average, respectively; Supplementary Fig. S3B–S3E). The MoMac cluster did not contain cells resembling monocytic or granulocytic MDSCs, when evaluated on the basis of the canonical MDSC marker expression (Supplementary Fig. S4A–S4C).

Next, we annotated the MoMac phenotypes within the MoMac cluster by mapping these cells to the cross-tissue single-cell atlas of human monocytes and macrophages (MoMac-VERSE; ref. 20; **Fig. 1G**; Supplementary Fig. S4D). The mapping revealed that the majority of the ovarian ascites MoMacs were TREM2 or IL4I1 macrophages (**Fig. 1H**; Supplementary Fig. S4E), which MoMac-VERSE authors describe as TAMs accumulating within human tumors (20). As we observed high abundancy of Clever-1$^+$ TAMs and individual variation in bexmarilimab responses, these data establish ovarian cancer ascites cells as a relevant human TIME model to investigate bexmarilimab mode-of-action.

Bexmarilimab triggers IFN signaling and CXCL10 secretion in ovarian ascites TAMs

We next sought to understand whether bexmarilimab treatment has distinct effects on TAM gene expression in R and NoR groups. GSEA revealed that IFNα and IFNγ signaling pathways were significantly upregulated in TAMs of the bexmarilimab-responsive ascites samples (**Fig. 2A** and **B**). Conversely, in the NoR group, bexmarilimab downregulated IFNα, IFNγ, IL6, and TNFα signaling (**Fig. 2A**). We used the scRNA-seq data to validate our original grouping of R and NoR ascites samples, and observed bexmarilimab altered macrophage IFN signaling in each patient sample to the direction expected on the basis of *MX1* induction (**Fig. 2C**). Similar but weaker changes in IFN signaling were also observed in CD8$^+$ T cells (**Fig. 2B** and **D**).

In line with the changes in TAM gene expression, higher levels of CXCL10 and CCL5 were observed in the culture supernatants of the R group (**Fig. 2E**). CCL5 and IFNγ-inducible CXCR3 ligands secreted by

Figure 3.

Bexmarilimab unresponsive ascites samples have abundant IL4I1 macrophages and higher baseline IFN signaling. **A,** Unsupervised hierarchical clustering of patient samples (NoR, $n = 3$; R, $n = 4$) based on immune cell type and subtype proportions. The cell type proportions were calculated for IgG4-treated ascites samples. Red color indicates higher cell type proportion in comparison with other samples. **B,** PCA of IgG4-treated ascites samples based on immune cell type and subtype proportions. A 3D scatter plot of first three principal components is shown. **C,** The contribution of each cell type on PC 1 and 3 is shown as an arrow pointing to loading scores on PC 1 and 3. Cell types with absolute loading score > 0.6 on PC 1 are labeled. Cell types with positive scores on PC 1 associate with NoR group and negative scores with R group. **D,** Most significant immune cell types found to differ between R and NoR group by PCA and unsupervised hierarchical clustering. Median ± IQR; Mann–Whitney U test. **E,** Comparison of ovarian ascites MoMac gene expression profiles between R ($n = 4$) and NoR ($n = 3$) group by GSEA performed on IgG4-treated samples. Red color indicates higher pathway-related gene expression in R group and blue in NoR group. **F,** Schematic summarizing the differences between R and NoR ascites samples. BEX, bexmarilimab; IgG4, isotype control for bexmarilimab.

myeloid cells, such as CXCL9 and CXCL10, cooperate to enhance T-cell recruitment into tumors (23). Macrophages appeared to be responsible for the CXCL10 secretion, as the MoMac cluster expressed the highest level of *CXCL10* among the ascites cells, and bexmarilimab increased the proportion of *CXCL10*$^+$ macrophages in the responding group (**Fig. 2F**; Supplementary Fig. S4F). To further investigate whether treating TAMs alone was sufficient for the elevated CXCL10 secretion, we isolated CD14$^+$ ascites cells and treated them with bexmarilimab. When treated alone, TAMs from the responsive group did not show similar induction of CXCL10 (**Fig. 2G**), suggesting that IFN secretion by other cell types is required for bexmarilimab-induced CXCL10 secretion. Taken together, these data highlight distinct immunological outcomes after bexmarilimab treatment and call for the identification of factors regulating these responses.

Bexmarilimab-responsive ascites samples have lower baseline IFN signaling and fewer IL4I1 macrophages

To investigate TIME features that could regulate the distinct bexmarilimab responses in the R and NoR groups, we subclustered the scRNA-seq immune cell clusters into immune cell subtypes (Supplementary Fig. S5A–S5H). Then, we evaluated patient-to-patient variation in proportions of these immune cell subtypes by performing unsupervised hierarchical clustering (**Fig. 3A**) and PCA (**Fig. 3B**). Both of these analyses revealed that the responders separated from the nonresponders based on the ascites immune cell composition. PCA loading plot and dendrogram of the hierarchical clustering both showed that DCs, IL4I1 macrophages, regulatory T cells (Treg), and MKI67$^+$ NK cells were more abundant in the NoR samples (**Fig. 3A** and**C**). The greatest differences between R and NoR group were observed in Treg, MKI67$^+$ NK cells, IL4I1 macrophages, and total macrophage proportions (**Fig. 3D**). IL4I1 macrophages are characterized by the expression of the secreted immunosuppressive enzyme IL4I1, which regulates the tumor microenvironment (TME) and T-cell activation by depleting amino acids and generating bioactive metabolites and by-products (24). In human macrophages, IL4I1 expression can be induced with IFNs and prolonged IFN exposure supports stronger IL4I1 induction (25).

Owing to the differences in macrophage populations, we next compared TAM phenotypes between the R and NoR groups. Both groups had similar levels of Clever-1 protein and bexmarilimab epitope on the surface of untreated MoMacs (Supplementary Fig. S5I–S5K). However, their gene expression profiles were significantly different, as IgG4-treated responder MoMacs showed lower levels of IFNα and IFNγ signaling (**Fig. 3E**). In summary, bexmarilimab-responsive TAMs have lower baseline expression of IFN response genes and lack the IL4I1 macrophage phenotype (**Fig. 3F**) that is induced by prolonged exposure to IFNs (20).

Chronic IFN priming suppresses the potency of bexmarilimab in primary macrophages

Because our results suggested an emerging role for IFNs in preventing bexmarilimab responses, we sought to validate this hypothesis in IFN-primed macrophages. For this we used a previously developed bexmarilimab potency assay measuring LPS responses in primary human macrophages after bexmarilimab treatment (26). The IFN priming was performed during macrophage differentiation from CD14$^+$ monocytes to facilitate chronic IFN exposure. We tested two different doses and three time periods of IFNγ priming (Supplementary Fig. S6A) and observed the highest IDO1 induction (an indicator of IFNγ-induced negative feedback) with negligible Clever-1 downregulation after 96 hours of priming with 20 ng/mL IFNγ concentration (Supplementary Fig. S6B–S6F). With the selected IFNγ concentration and priming length, we primed human monocytes with IFNγ or IFNα2, treated them with bexmarilimab and measured the strength of subsequent macrophage activation upon TLR4 ligation with LPS (**Fig. 4A**). Bexmarilimab increased the secretion of TNFα after LPS-stimulus, but preexposure to IFNγ inhibited the bexmarilimab-induced TNFα release (**Fig. 4B**). To investigate the timescale of this inhibitory effect, we compared acute (2 hours + 24 hours) and chronic (96 hours + 24 hours) IFNγ priming; we observed stronger inhibition of TNFα secretion upon chronic IFNγ priming (**Fig. 4C**). A similar inhibition of bexmarilimab-induced immune activation was observed with acute and chronic IFNα2 priming, but the decrease in TNFα secretion was weaker than with IFNγ (median fold change 0.94 vs. 0.79; **Fig. 4D**). Downregulation of Clever-1 is unlikely to account for the inhibition, as a significant proportion of Clever-1 expression remained on the cells and IFNα2 decreased Clever-1 expression more despite inhibiting TNFα secretion less (**Fig. 4E** and **F**; and Supplementary Fig. S6G). Altogether, these data show that chronic exposure to IFNs prevents macrophages from being further activated by bexmarilimab.

Bexmarilimab nonresponsive patients in the MATINS trial have more IL4I1$^+$ stromal cells

Having observed fewer IL4I1 macrophages in bexmarilimab-responding ovarian ascites samples, we investigated whether chronic IFN signaling associated with IL4I1 expression would similarly correlate with the lack of bexmarilimab response within the patient TME. For this, we stained for IL4I1 on pre–bexmarilimab-treatment tumor biopsies from the MATINS trial. The biopsies from patients with disease control (DCR) and without disease control (non-DCR) during subsequent bexmarilimab therapy represented five different types of advanced solid tumors. In the TME, IL4I1 is mainly expressed by TAMs and to a lesser extent by DCs and Tregs in the investigated cancer types (27, 28), and we observed IL4I1 to highly co-localize with CD68$^+$ macrophages in breast cancer when testing signal specificity (Supplementary Fig. S7A and S7B). Quantification of the IL4I1 staining showed that non-DCR patients had a tendency for higher IL4I1$^+$ cell density in the tumor stroma [median 81.7 cells/mm^2; interquartile range (IQR), 63.8–135.4] in comparison with DCR patients (median 41.9 cells/mm^2; IQR, 13.1–134.8; **Fig. 4G** and **H**), suggesting that IFNs could have an impact in bexmarilimab response within solid tumors.

Discussion

Rewiring TAMs to support antitumor immunity, potentially in combination with T cell–based therapies, may generate the next wave of cancer immunotherapies (2). With opposing roles of different TAM subsets in cancer promotion and immune activation, targeting the TAM pool as a whole will not yield optimal results (4, 5). Single-cell approaches have revealed high intratumoral and between-patient heterogeneity in TAM phenotypes, and thus highlighted the importance of identifying clinically relevant and selectively targetable TAM subsets (3). On the basis of preclinical and early clinical evidence, Clever-1 expression defines one such TAM subset, as the immunosuppressive functions of Clever-1 on monocytes and macrophages can be blocked with the Clever-1–specific antibody bexmarilimab to activate adaptive immunity (11, 12). However, it is currently unknown which factors regulate bexmarilimab treatment responses in human TAMs and determine therapy outcome in cancer patients. Here, we addressed these questions in *ex vivo*–treated ovarian ascites cells using scRNA-seq.

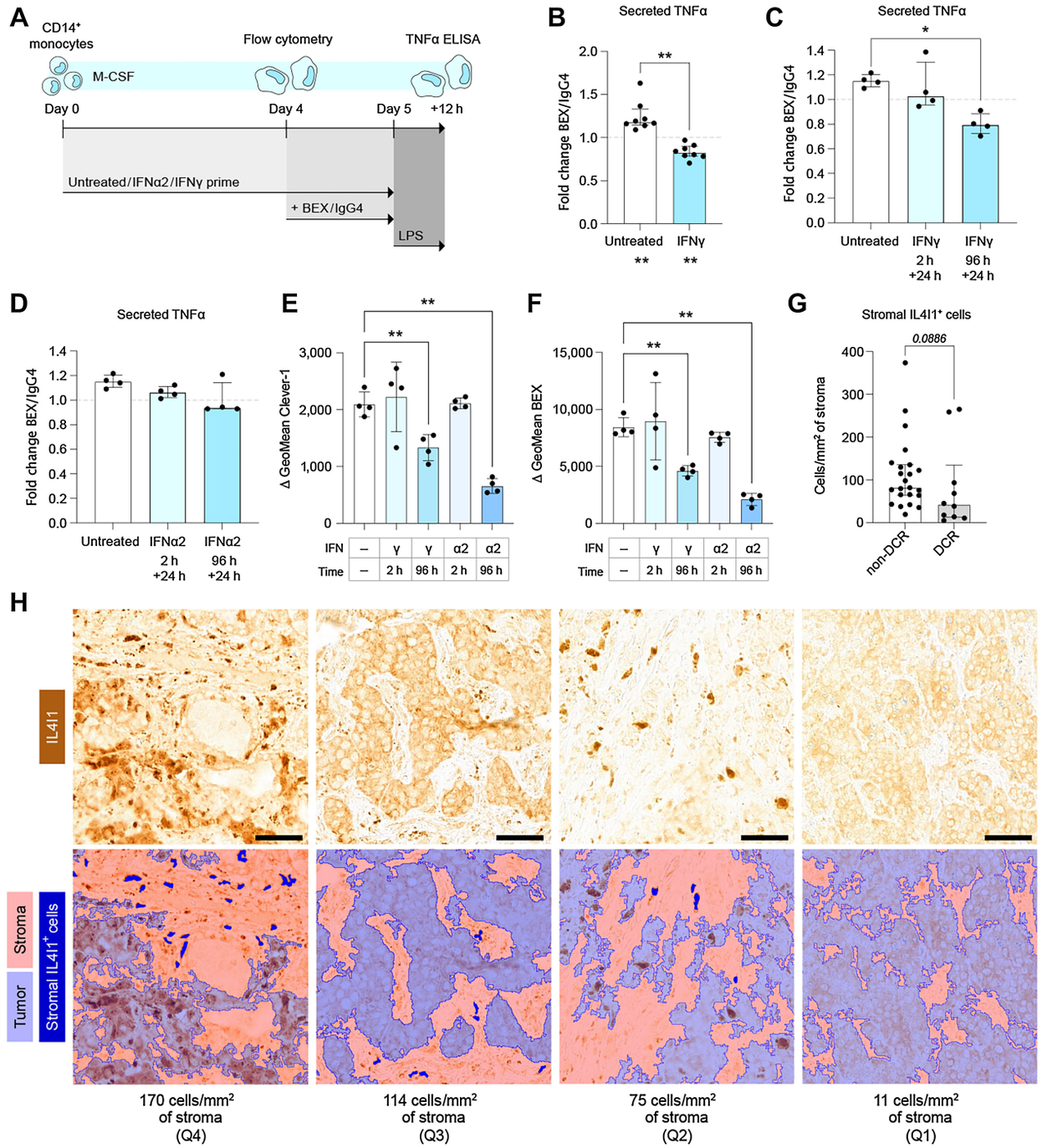

Figure 4.

Chronic IFN priming inhibits further macrophage activation by bexmarilimab. **A,** Schematic showing timeline for primary human macrophage differentiation and simultaneous IFN priming, followed by bexmarilimab treatment and measurement of LPS response. **B,** TNFα secretion after bexmarilimab treatment in unprimed or IFNγ-primed macrophages ($n = 8$ healthy donors, two independent experiments). Median ± IQR, Wilcoxon signed rank tests for each group and Wilcoxon matched-pairs signed rank test. **C** and **D,** TNFα secretion after bexmarilimab treatment in macrophages primed with IFNγ (**C**) or IFNα2 (**D**). Acute priming (2 hours before and 24 hours during antibody treatment) and chronic priming (96 hours before and 24 hours during antibody treatment) are shown for $n = 4$ healthy donors. Median ± IQR, Friedman test followed by Dunn test. **E** and **F,** Macrophage Clever-1 expression (**E**) and abundancy of available bexmarilimab epitope (**F**) on day 4 after no priming, 2 hours, or 96 hours of indicated IFN priming. Mean ± SD, RM one-way ANOVA followed by Dunnett test. **G,** IL4I$^+$ stromal cell abundancy in pretreatment biopsies collected from patients with (DCR, $n = 10$) and without (non-DCR, $n = 23$) disease control during bexmarilimab therapy in MATINS trial. Median ± IQR; Mann–Whitney U test. **H,** Representative images of MATINS pretreatment biopsies displaying a range of different stromal IL4I1$^+$ cell densities (image per each quartile of cell densities). IL4I1 staining (top), detected tumor areas (bottom; light blue), detected stromal areas (bottom; light red) and detected stromal IL4I1$^+$ cells (bottom; dark blue) are shown. Scale bars, 50 μm. *, $P < 0.05$; **, $P < 0.01$; BEX, bexmarilimab; IgG4, isotype control for bexmarilimab.

Our in-depth *ex vivo* characterization of bexmarilimab activity on ovarian ascites cell populations showed that bexmarilimab upregulated the expression of both type I and type II IFN responsive genes and CXCL10 secretion. IFN signaling has complex roles in the TME, but supports $CD8^+$ T-cell activation and Th1 responses upon acute induction (29, 30). CXCL10 is an IFNγ-inducible chemokine and macrophage-derived CXCL10 promotes T-cell migration into tumors and ICI therapy efficacy (31). In ovarian cancer, an increase in $CXCL10^+$ TAMs has been shown to be beneficial, as they are associated with antitumor immunity and responsiveness to immunotherapy (32). We did not observe these effects while treating $CD14^+$ ascites cells with bexmarilimab in isolation, which indicates that other cell types such as $CD8^+$ T cells, Th1 cells and NK cells constitute the main IFN source in the TME (29). As bexmarilimab's parent antibody (3–372) can enhance IFNγ secretion in antigen-specific recall assays performed with PBMCs (10), it seems that bexmarilimab treatment first activates macrophages, which then become capable of inducing IFN secretion by surrounding immune cells. Potential mechanisms for this macrophage-mediated immune activation have been reported previously, as Clever-1 disruption slows down antigen degradation in favor of antigen presentation (12), induces TNFα (26) and IL12 secretion, and activates NF-κB and mTOR signaling in macrophages (11).

The antitumor effects of bexmarilimab were, however, only evident in those samples that did not show prior IFN activation. Unlike acute IFN signaling, chronic IFN exposure is known to induce negative feedback mechanisms, that inhibit overactivation of the immune system and promote immunosuppression instead (29). One such immunosuppressive molecule induced by chronic IFNγ exposure in macrophages is IL4I1 (25), which we observed to be elevated in bexmarilimab nonresponsive ascites samples and patients not benefitting from bexmarilimab therapy. Upon *in vitro* validation, we observed chronic IFNγ priming of macrophages to dampen the ability of bexmarilimab to increase TLR4-induced TNFα secretion. Because IFNγ priming has been shown to superinduce TNFα after LPS by disrupting IL10-inducible gene expression (33), it is possible that subsequent bexmarilimab treatment promotes feedback mechanisms to inhibit overactivation of the cell. Moreover, IFNγ can also repress LPS-activated pathways related to lipid and iron metabolism pathways (33). Our previous analyses of bexmarilimab mode-of-action on monocytes and macrophages show that it blocks tolerogenic gene expression related to LXR/RXR and PPAR pathways and specifically inhibits the interaction of Clever-1 with the transferrin receptor (12). Thus, there is also a possibility that IFNγ priming could interfere with bexmarilimab activity via these two pathways. In any case, these results strongly imply that bexmarilimab therapy would exhibit highest efficacy in non-inflamed, immunologically cold tumors characterized by low preexisting IFN signaling. Activating TAMs in these cold tumors with bexmarilimab can upregulate IFNγ signaling and T-cell recruitment, and therefore make these tumors more susceptible to T cell–based immunotherapies.

In conclusion, we demonstrate here that modulating human TAMs with bexmarilimab stimulates tumor-associated leukocytes to support adaptive immunity in cancer. This immune modulation was exclusively observed in TAMs lacking previous exposure to IFNγ. Our results thus support the treatment of immunologically cold tumors with bexmarilimab to activate antitumoral immunity, and can potentially guide patient selection in future clinical trials.

Authors' Disclosures

P. Bono reports personal fees from Faron Pharmaceuticals during the conduct of the study; personal fees from MSD and Oncorena; personal fees from TILT Therapeutics outside the submitted work; and stock ownership at Faron Pharmaceuticals (spouse). J. Hynninen reports grants from EU Horizon 2020 during the conduct of the study. M. Hollmén reports nonfinancial support and other support from Faron Pharmaceuticals; grants from Academy of Finland, Cancer Foundation; grants from Sigrid Juselius Foundation during the conduct of the study; other support from Faron Pharmaceuticals outside the submitted work; and is currently employed by Faron Pharmaceuticals. No disclosures were reported by the other author.

Authors' Contributions

J.H. Rannikko: Conceptualization, data curation, software, formal analysis, funding acquisition, validation, investigation, visualization, methodology, writing–original draft, writing–review and editing. **P. Bono:** Resources, investigation, project administration, writing–review and editing. **J. Hynninen:** Resources, data curation, funding acquisition, investigation, project administration, writing–review and editing. **M. Hollmén:** Conceptualization, resources, supervision, funding acquisition, investigation, methodology, writing–original draft, project administration, writing–review and editing.

Acknowledgments

We thank the patients and healthy volunteers donating tissues or cells for our study as well as the participants, investigators, and research team of the MATINS trial. We also want to thank Teija Kanasuo, Sari Mäki, Mari Parsama, Chantal Harth, and Oliver Hollmén for excellent technical assistance. The study was supported by Cell Imaging and Cytometry Core, Single Cell Omics Core and Finnish Functional Genomics Centre, University of Turku, Åbo Akademi and Biocenter Finland.

This study was funded by Faron Pharmaceuticals (Turku, Finland), European Union's Horizon 2020 research and innovation program (ID 960914 and ID 965193), the Academy of Finland (to M. Hollmén), Cancer Foundations (to M. Hollmén and J. H. Rannikko), the Sigrid Jusélius Foundation (to M. Hollmén), Orion Research Foundation (to J.H. Rannikko) and the Paulo Foundation (to J.H. Rannikko).

Note

Supplementary data for this article are available at Cancer Immunology Research Online (http://cancerimmunolres.aacrjournals.org/).

Received April 24, 2023; revised September 11, 2023; accepted October 31, 2023; published first December 1, 2023.

References

1. Sharma P, Siddiqui BA, Anandhan S, Yadav SS, Subudhi SK, Gao J, et al. The next decade of immune checkpoint therapy. Cancer Discov 2021;11:838–57.
2. Goswami S, Anandhan S, Raychaudhuri D, Sharma P. Myeloid cell-targeted therapies for solid tumors. Nat Rev Immunol 2023;23:106–20.
3. Pittet MJ, Michielin O, Migliorini D. Clinical relevance of tumor-associated macrophages. Nat Rev Clin Oncol 2022;19:402–21.
4. Cassetta L, Pollard JW. Targeting macrophages: therapeutic approaches in cancer. Nat Rev Drug Discov 2018;17:887–904.
5. Cassetta L, Pollard JW. A timeline of tumor-associated macrophage biology. Nat Rev Cancer 2023;23:238–57.
6. Bercovici N, Guérin MV, Trautmann A, Donnadieu E. The remarkable plasticity of macrophages: a chance to fight cancer. Front Immunol 2019;10:1563.
7. Chen DS, Mellman I. Elements of cancer immunity and the cancer-immune set point. Nature 2017;541:321–30.
8. Hollmén M, Figueiredo CR, Jalkanen S. New tools to prevent cancer growth and spread: a 'Clever' approach. Br J Cancer 2020;123:501–9.
9. Kzhyshkowska J. Multifunctional receptor stabilin-1 in homeostasis and disease. ScientificWorldJournal 2010;10:2039–53.
10. Palani S, Elima K, Ekholm E, Jalkanen S, Salmi M. Monocyte stabilin-1 suppresses the activation of Th1 lymphocytes. J Immunol 2016;196:115–23.

11. Viitala M, Virtakoivu R, Tadayon S, Rannikko J, Jalkanen S, Hollmén M. Immunotherapeutic blockade of macrophage Clever-1 reactivates the $CD8^+$ T-cell response against immunosuppressive tumors. Clin Cancer Res 2019;25: 3289–303.
12. Virtakoivu R, Rannikko JH, Viitala M, Vaura F, Takeda A, Lönnberg T, et al. Systemic blockade of clever-1 elicits lymphocyte activation alongside checkpoint molecule downregulation in patients with solid tumors: results from a phase I/II clinical trial. Clin Cancer Res 2021;27:4205–20.
13. Bexmarilimab-induced macrophage activation leads to treatment benefit in solid tumors: the phase I/II MATINS trial [Internet]. 2023. Available from: https://doi.org/10.1101/2023.04.17.23288693.
14. Hao Y, Hao S, Andersen-Nissen E, Mauck WM, Zheng S, Butler A, et al. Integrated analysis of multimodal single-cell data. Cell 2021;184:3573–87.
15. McGinnis CS, Murrow LM, Gartner ZJ. DoubletFinder: doublet detection in single-cell RNA sequencing data using artificial nearest neighbors. Cell Syst 2019; 8:329–37.
16. Hashimoto S, Suzuki T, Dong HY, Nagai S, Yamazaki N, Matsushima K. Serial analysis of gene expression in human monocyte-derived dendritic cells. Blood 1999;94:845–52.
17. Goudot C, Coillard A, Villani AC, Gueguen P, Cros A, Sarkizova S, et al. Aryl hydrocarbon receptor controls monocyte differentiation into dendritic cells versus macrophages. Immunity 2017;47:582–96.
18. Bronte V, Brandau S, Chen SH, Colombo MP, Frey AB, Greten TF, et al. Recommendations for myeloid-derived suppressor cell nomenclature and characterization standards. Nat Commun 2016;7:12150.
19. Hegde S, Leader AM, Merad M. MDSC: markers, development, states, and unaddressed complexity. Immunity 2021;54:875–84.
20. Mulder K, Patel AA, Kong WT, Piot C, Halitzki E, Dunsmore G, et al. Cross-tissue single-cell landscape of human monocytes and macrophages in health and disease. Immunity 2021;54:1883–900.
21. Gu Z, Eils R, Schlesner M. Complex heatmaps reveal patterns and correlations in multidimensional genomic data. Bioinformatics 2016;32:2847–9.
22. Bankhead P, Loughrey MB, Fernández JA, Dombrowski Y, McArt DG, Dunne PD, et al. QuPath: open source software for digital pathology image analysis. Sci Rep 2017;7:16878.
23. Dangaj D, Bruand M, Grimm AJ, Ronet C, Barras D, Duttagupta PA, et al. Cooperation between constitutive and inducible chemokines enables T cell engraftment and immune attack in solid tumors. Cancer Cell 2019; 35:885–900.
24. Zeitler L, Murray PJ. IL4i1 and IDO1: oxidases that control a tryptophan metabolic nexus in cancer. J Biol Chem 2023;299:104827.
25. Marquet J, Lasoudris F, Cousin C, Puiffe ML, Martin-Garcia N, Baud V, et al. Dichotomy between factors inducing the immunosuppressive enzyme IL-4-induced gene 1 (IL4I1) in B lymphocytes and mononuclear phagocytes. Eur J Immunol 2010;40:2557–68.
26. Hollmén M, Maksimow M, Rannikko JH, Karvonen MK, Vainio M, Jalkanen S, et al. Nonclinical characterization of bexmarilimab, a Clever-1-targeting antibody for supporting immune defense against cancers. Mol Cancer Ther 2022;21: 1207–18.
27. Carbonnelle-Puscian A, Copie-Bergman C, Baia M, Martin-Garcia N, Allory Y, Haioun C, et al. The novel immunosuppressive enzyme IL4I1 is expressed by neoplastic cells of several B-cell lymphomas and by tumor-associated macrophages. Leukemia 2009;23:952–60.
28. Ramspott JP, Bekkat F, Bod L, Favier M, Terris B, Salomon A, et al. Emerging role of IL-4-induced gene 1 as a prognostic biomarker affecting the local T-cell response in human cutaneous melanoma. J Invest Dermatol 2018;138:2625–34.
29. Gocher AM, Workman CJ, Vignali DAA. Interferon-γ: teammate or opponent in the tumor microenvironment? Nat Rev Immunol 2022;22:158–72.
30. Boukhaled GM, Harding S, Brooks DG. Opposing roles of Type I interferons in cancer immunity. Annu Rev Pathol 2021;16:167–98.
31. House IG, Savas P, Lai J, Chen AXY, Oliver AJ, Teo ZL, et al. Macrophage-derived CXCL9 and CXCL10 are required for antitumor immune responses following immune checkpoint blockade. Clin Cancer Res 2020;26:487–504.
32. Ardighieri L, Missale F, Bugatti M, Gatta LB, Pezzali I, Monti M, et al. Infiltration by CXCL10 secreting macrophages is associated with antitumor immunity and response to therapy in ovarian cancer subtypes. Front Immunol 2021;12:690201.
33. Kang K, Bachu M, Park SH, Kang K, Bae S, Park-Min KH, et al. IFN-γ selectively suppresses a subset of TLR4-activated genes and enhancers to potentiate macrophage activation. Nat Commun 2019;10:3320.